Ultrafast X-ray Diffraction Theory

Jianshu Cao* and Kent R. Wilson

Department of Chemistry and Biochemistry, University of California—San Diego, La Jolla, California 92093-0339

Received: April 29, 1998; In Final Form: July 10, 1998

Time-resolved X-ray diffraction patterns can be inverted to obtain photoinduced dynamics without resorting to additional and often unknown information (e.g., potential energy surfaces), as required in optical probe experiments. In order to interpret ultrafast X-ray diffraction measurements, we consider several time scales in X-ray experiments involving elastic versus inelastic scattering, quantum interference among electronic states, physical implications of temporal- and spatial-averaging, and the coherence of X-ray beams. On the basis of these considerations, it is shown that inelastic scattering can be employed to measure the time dependence of electron correlation and the nonadiabatic effects in curve crossing. As in the snapshot approach, the Born−Oppenheimer approximation and the independent atom model are adopted such that molecular dynamics can be directly probed without explicit reference to electron density. In addition, we show that (i) the inversion for a cylindrically symmetric sample can be simplified by looking along a specific direction and (ii) that by means of molecular "π pulses" the excited state dynamics can be isolated without contamination from the ground electronic state. With certain modifications, the time-dependent analysis presented here can be applied to other experimental methods including electron diffraction and X-ray absorption (chemical shifts, near-edge, and EXAFS).

I. Introduction

Our knowledge of evolving molecular structures is usually obtained through time-resolved or frequency-resolved optical experiments, most notablely using ultrafast optical pump-probe pulses. Unfortunately, except for a few favorable cases of small molecules, such optical probe measurements can seldom lead to the desired real-time picture of where the atoms and electrons are in real space because the inversion of optical observables to molecular dynamics requires prior knowledge such as potential energy surfaces and linear or higher order transition dipole moments and polarizabilities. Ever since its discovery at the turn of the century,[1] X-ray diffraction has been widely used to measure the equilibrium molecular structures of a large number of molecules including polymers and proteins. Unlike optical spectroscopy, time-resolved X-ray diffraction[2−7] directly measures electronic and nuclear motions during chemical and physical processes without resorting to any additional and often unknown information. In addition to X-ray diffraction, ultrafast extended X-ray absorption fine structure (EXAFS) and the near edge spectrum can be used to detect changes in local environments, such as bond motions and solvation dynamics,[8] and time-resolved chemical shifts of atomic absorption threshold can in principle be used to detect charge transfer or the oxidation state of chosen atoms. Thus, ultrafast X-ray diffraction and absorption techniques may soon emerge as powerful ways to observe the evolution of chemical reactions, the dynamics of biological systems, and the kinetics of structured materials.

Figure 1 illustrates a time-resolved X-ray diffraction experiment where the dynamics of a sample is initiated by an ultrafast optical laser pulse and then probed by an ultrafast X-ray pulse at various delay times. As real-space configurations can be inverted from X-ray diffraction patterns and then recorded as a function of delay time, one can follow the course of chemical and physical processes initiated by the optical pump pulse in real time and real space.[9−11] From a simple viewpoint, ultrafast X-ray diffraction can be understood as taking snapshots of nonstationary nuclear configurations. This snapshot approach is based on the assumption that X-ray scattering is elastic with respect to electronic degrees of freedom and nuclear motion is frozen during the X-ray scattering. Such an ultrafast X-ray experiment should have sub-picosecond temporal resolution for

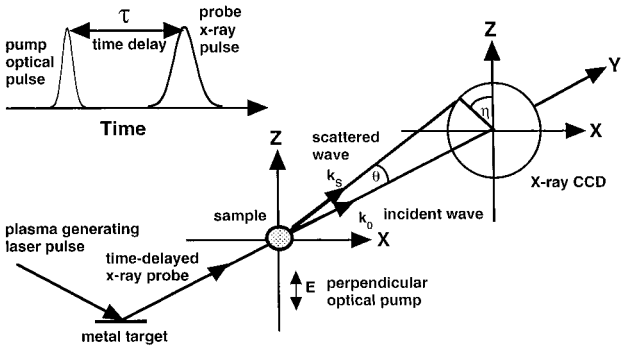

Figure 1. An illustration of ultrafast X-ray diffraction. The X-ray pulse is generated by a dense, high energy plasma produced on a metal surface by illumination with an ultrafast high intensity optical pulse, which is delayed by τ with respect to the pump pulse. In the perpendicular experimental arrangement, the polarization vector ϵ of the optical pump pulse (Z axis) is perpendicular to the incident wave vector $\mathbf{k}_o$ of the X-ray probe pulse (Y axis). The incident X-ray photons propagating along the Y axis scatter at angle θ with respect to $\mathbf{k}_o$ and at azimuthal angle η with respect to ϵ. The scattering vector $\mathbf{s}$ is the difference between the incident and scattered wave vectors, $\mathbf{s} = \mathbf{k}_o - \mathbf{k}_s$.

* Corresponding author. Present address: Department of Chemistry, Massachusetts Institute of Technology, Cambridge, MA 02139.

10.1021/jp982054p CCC: $15.00
Published on Web 10/29/1998

vibrational motions or bond making and breaking and subangstrom spatial resolution for internuclear distance.

The ultrafast X-ray method is built on the same concept as the ultrafast optical pump−probe technique except that X-ray radiation is used for probing instead of optical pulses. The appealing prospect of real time dynamics in real space has motivated an increasing number of ultrafast X-ray diffraction and absorption experiments.[12,3−8] In addition, theorists have begun to explore various possible applications of the time-resolved X-ray techniques through numerical examples.[9,10] However, the theoretical basis of time-resolved X-ray diffraction is not fully elucidated in these studies. As the temporal resolution of X-ray detection approaches the limit of resolving electronic dynamics in addition to nuclear dynamics, a more complete and rigorous approach is required. In this paper, we formulate ultrafast X-ray diffraction theory from first principles, explore the possibilities of resolving electronic coherence in atomic systems and curve crossing in molecular systems, and finally reduce it to more conventional expressions appeared in the snapshot approach.[10]

This paper is a continuation of the theoretical effort to explore time-resolved X-ray diffraction, most notablely in the recent paper by Ben-nun et al.[10] Although some results have appeared in the previous paper, this work includes several new contributions to time-dependent X-ray diffraction theory. Most importantly, by virtue of the Wigner representation of X-ray pulses, we formulate a general ultrafast diffraction theory on the intensity level and then reduce it to various limits including coherent and incoherent X-ray sources, long and short X-ray pulses, and elastic and inelastic scattering. Consequently, the starting point in the previous paper (i.e., eq 2.1) becomes an end-result of our general formalism and we are able to derive expressions for cases beyond the assumptions used in the previous paper, such as nonadiabatic nuclear dynamics and electronic coherence. For the completeness of the paper, we briefly rephrase the Born−Oppenheimer approximation and the independent atom model, as introduced in the previous paper. Nevertheless, new aspects in the construction of molecular dynamics from X-ray diffraction are developed: (i) the analysis of the angular distribution of X-ray diffraction patterns beyond linear optical excitation, (ii) the Implication for the inversion procedure due to cylindrical symmetry, (iii) the removal of the ground state contribution by using molecular π pulses. The numerical example in this paper uses strong-field excitation of molecular π pulses and hence differs from the previous calculation. In the strong excitation regime, the angular distribution is coupled to the radial distribution and the transformation between the real-space distribution and diffraction pattern becomes more challenging than for the weak response regime. In short, the paper represents more general and quantitative theoretical developments along the line of earlier work.

Unified ultrafast X-ray diffraction theory is derived in section II with detailed analysis of various time scales and their effects on X-ray temporal and spatial resolution. Applications to electronic dynamics are discussed in section III and the relation of X-ray measurements to diagonal and off-diagonal reduced electron density matrix elements is clarified. In section IV, we demonstrate that nonadiabatic effects in molecular systems can be observed in diffraction patterns with femtosecond resolution. Under the Born−Oppenheimer approximation and the independent atom model, molecular dynamics can be directly probed without reference to electron density. Accurate inversion of the diffraction pattern of an initially isotropic sample to the internuclear distance distribution is shown to be greatly simplified due to the cylindrical symmetry of such optically excited molecular systems. Furthermore, by applying recent techniques of population inversion of molecular systems by positively chirped strong field short pulses,[13,14] the excited state dynamics can in principle be isolated using molecular "π pulses" and investigated without interference from the ground state distribution. We present a simple numerical example in section V and conclude in section VI.

II. Theoretical Considerations

A. General Formalism. An optical pump pulse produces a nonstationary wave function, $\psi(t)$, which is then detected by an X-ray probe pulse, whose electric field is $E(t)$. The general starting point for X-ray diffraction theory is Born's perturbative theory for quantum scattering.[15] To first order in the scattering potential, the X-ray scattering operator is defined as

$$L(\mathbf{s}) = \sum_{\mu} e^{i\mathbf{s}\cdot\mathbf{r}_\mu} \tag{1}$$

where $\mathbf{r}_\mu$ is the coordinate of the μth electron and the summation over μ extends to all electrons in the scattering center. The scattering vector $\mathbf{s}$ is the difference between the incident wave vector $\mathbf{k}_o$, and the scattered wave vector $\mathbf{k}_s$ (i.e., $\mathbf{s} = \mathbf{k}_o - \mathbf{k}_s$). Then, the scattering amplitude into a final state n can be expressed as

$$f_n(\mathbf{s}) = \int dt\, E(t)\langle\phi_n| e^{i\epsilon_n t + i\omega_s t} L(\mathbf{s}) e^{-i\omega_o t}|\psi(t)\rangle \tag{2}$$

where irrelevant prefactors are ignored, ϕ_n is a final eigenstate wave function with eigenenergy ϵ_n, ω_o and ω_s are the incident and scattered photon frequencies, respectively, and $\hbar$ is set to unity here and elsewhere. In this paper, bold fonts are used to denote three-dimensional vectors and normal fonts are used to denote ordinary variables. It follows that the total scattering intensity is given by

$$I(\mathbf{s}) = \sum_n |f_n(\mathbf{s})|^2 \tag{3}$$

where the summation over the final states does not necessarily extend over all n, but depends on factors such as the accessible detection range in the diffraction measurement, as is discussed below.

Substituting eq 2 into eq 3, we obtain

$$I(\mathbf{s}) = \sum_n \int\int dt dt' E(t) E^*(t') \langle\psi(t')| e^{i\omega_o t'} L^+(\mathbf{s}) e^{-i\epsilon_n t' - i\omega_s t'} |\phi_n\rangle\langle\phi_n| e^{i\epsilon_n t + i\omega_s t} L(\mathbf{s}) e^{-i\omega_o t}|\psi(t)\rangle$$

where L^+ is the complex conjugate of the scattering operator in eq 1. If we assume an X-ray beam, for example from a laser-driven plasma, consisting of numerous spontaneous emission events,[16,5,6] an additional average over the photon statistics, $\langle\cdots\rangle_{ph}$, must be carried out on the intensity level. To simplify the analysis, we define a new set of variables as $\tau = (t + t')/2$ and $\delta = t' - t$ and introduce the Wigner transform $F(\tau,\omega)$ of the incident X-ray pulse

$$\langle E(t)E^*(t')\rangle_{ph} = \frac{1}{2\pi}\int d\omega e^{-i\omega\delta} F(\tau,\omega) \tag{4}$$

where the carrier frequency ω_0 has been removed from the transformation. For most practical applications, $F(\tau,\omega)$ can be

factorized as

$$\mathrm{F}(\tau,\omega) = \mathrm{A}(\tau)\mathrm{P}(\omega) \tag{5}$$

where $A(\tau)$ is the temporal envelope with its width given by the pulse duration τ_{dur} and $P(\omega)$ is the power spectrum with its width determined by the pulse bandwidth Γ and other factors discussed below. To proceed, we expand the nonstationary wave function $\psi(t)$ in eigenstate space as $\psi(t) = \sum_i c_i e^{-i\omega_i t}\phi_i$ with ω_i being the eigen frequency of ϕ_i and, similarly, $\psi(t') = \sum_j c_j e^{-i\omega_j t'}\phi_j$, with ω_j being the eigen frequency of ϕ_j. Then, eq 4 can be recast as

$$\mathrm{I}(\mathbf{s}) = \sum_{\mathrm{ij}} B_{ij} C_{ij}(\mathbf{s}) \tag{6}$$

where B_{ij} results from the integral over τ

$$B_{ij} = c_i c_j \int A(\tau) e^{-i(\omega_i - \omega_j)\tau}\, d\tau \tag{7}$$

and C_{ij} results from the integral over δ

$$C_{ij}(\mathbf{s}) = \sum_n \langle\phi_j|L^+|\phi_n\rangle\langle\phi_n|L|\phi_i\rangle P[\omega_s - \omega_0 + \epsilon_n - (\epsilon_i + \epsilon_j)/2] \tag{8}$$

Evidently, B_{ij} represents a temporal average which imposes a constraint on the time-resolved detection of the photon-induced wave packet, whereas C_{ij} represents a spectral average which imposes a constraint on the summation over the final states n. Since eqs 6−8 are written in terms of physical quantities such as scattering intensity and X-ray intensity, the wave function representation in the above equations can be naturally transformed into a density matrix representation.

In standard time-independent X-ray diffraction theory, scattering intensity is simply the square of scattering amplitude. With time-resolved diffraction, the expression for scattering intensity is the combined result of several time-scale considerations, including coherence of X-ray sources and time averaging, quantum interference among eigenstates, elasticity and spatial averaging. The two expressions in eqs 7 and 8 constitute the basis for theoretical considerations of time-resolved X-ray diffraction and will be analyzed at length in the following subsections.

B. X-ray Coherence and Temporal-Averaging. The factorization in eq 5 holds for the two general cases of electric fields: coherent transformed-limited X-ray pulses and trains of incoherent X-ray emission. For a coherent X-ray source, the pulse duration τ_{dur} and bandwidth Γ are related via $\tau_{\mathrm{dur}} \propto 2\pi$. Consequently, the conditions introduced in eqs 7 and 8 are not independent; in other words, the analysis of time-resolved X-ray diffraction can be carried out both on the intensity level and on the amplitude level. This can be easily understood because the additional average on photon statistics in eq 4 is irrelevant for coherent X-ray sources.

For incoherent X-ray emission, the pulse duration τ_{dur} and bandwidth Γ are two independent parameters related to two different aspects of time-resolved X-ray diffraction. In the limit that the X-ray bandwidth Γ is much larger than the bandwidth of the relevant spectrum of the molecular system being probed, one can ignore the effect of the spectral distribution in eq 8, (i.e., $P(\omega) = 1$). Then, the two expressions in eqs 7 and 8 can be combined to yield

$$I = \sum_n \int \mathrm{d}t\, A(t)\langle\psi(t)|L^+|\phi_n\rangle\langle\phi_n|L|\psi(t)\rangle \tag{9}$$

where, for simplicity of notation, the scattering vector **s** is omitted as in the rest of the section. Thus, the time averaging on the amplitude level in eq 2 is reduced to a time averaging on the intensity level in eq 9, as a result of the incoherence of the spontaneous X-ray emission.

The above results can also be obtained from time-domain analysis. Under the assumption that the average coherence time of X-ray photons τ_{coh} is significantly shorter than any dynamical time scale of the molecular system, we have the incoherent X-ray result

$$\langle E(t)E(t')\rangle_{\mathrm{ph}} = \delta(t - t')A(t) \tag{10}$$

and hence the scattering intensity in eq 9. In fact, the expression $P(\omega) = 1$ and eq 10 are the spectral and temporal representations of the same physical limit. In comparison, for coherent X-ray sources, the integral over time can be carried out on the electric field level and the scattering intensity is calculated directly from the scattering amplitude without invoking eq 10.

C. Pulse Duration and Interference. To understand the time-averaging in eq 7, we assume a Gaussian profile for the X-ray pulse profile $A(t) = \exp(-t^2/\tau_{\mathrm{dur}}^2)$. Then the contribution to the scattering intensity from the cross term of ϕ_i and ϕ_j takes the form of

$$B_{ij} \propto \exp\left[-\frac{1}{2}(\omega_i - \omega_j)^2\tau_{\mathrm{dur}}^2\right] \tag{11}$$

which effectively introduces a constraint on the summation of pairs of eigenstates. Equation 11 indicates the interference between component eigenstates in $\psi(t)$ is smeared out by averaging over the X-ray pulse when $|\omega_i - \omega_j|\tau_{\mathrm{dur}} > 1$. This result is obtained directly from eq 7 and therefore is valid regardless of the coherence of the X-ray source. Since the eigen frequency difference $\omega_i - \omega_j$ represents the inverse of the time scale of the quantum dynamics, eq 11 indicates that an incoherent X-ray pulse cannot detect quantum coherence on a time scale much shorter than the pulse duration and that the interference between (i, j) quantum states will thus only be seen in the diffraction intensity when $|\omega_i - \omega_j|\tau_{\mathrm{dur}}$ is sufficiently small. This is a consequence of the Heisenberg uncertainty principle: the shorter the X-ray pulse, the faster phase modulation it detects.

D. Dynamic Response, Elasticity, and Spatial-Averaging. As indicated in eq 8, the X-ray power spectrum imposes a limit on the summation over the final states ϕ_n in eq 9, that is, $|\epsilon_n - (\epsilon_i + \epsilon_j)/2| < \delta\epsilon$, where a dynamic response range, $\delta\epsilon$, is introduced. In reality, this important parameter is the combined effect of the energy response of X-ray detection, the range of the scattered states with nonvanishing scattering amplitudes, and the bandwidth of the incident X-ray pulse. With the consideration of pulse duration and dynamic response, the general expression for the scattering intensity in eq 9, upon expanding $\psi(t) = \sum_i c_i(t)\phi_i$, becomes

$$I = \sum_{(i,j,n)} \int \mathrm{d}t A(t) c_i^*(t) c_j(t) f_{ni}^+ f_{nj} \tag{12}$$

where the summation over pairs of initial states (i, j) is constrained by the X-ray pulse duration as indicated in eq 11, the summation over n is constrained by the dynamic response as indicated above, and f_{ni} is the scattering amplitude defined as $f_{ni} = \langle\phi_n|L|\phi_i\rangle$.

The physical meaning of the dynamic response becomes evident when it is related to the effective elasticity of X-ray

scattering. To see this, consider two limiting cases of X-ray scattering. If the dynamic response is much smaller than the energy gap of the system (i.e., the internal energy spacing) then the X-ray scattering is elastic and eq 12 becomes

$$I_{\mathrm{el}} = \int \mathrm{d}t A(t) \sum_i |c_i f_i|^2 \tag{13}$$

where the spatial averaging is carried out on the amplitude level with eigenstates (i.e., $f_i = \langle \phi_i | L | \phi_j \rangle$). Since information as to phase differences among initial states is lost, the diffraction intensity does not reveal the time dependence of $\psi(t)$. On the other hand, if the dynamic response is much larger than the range of spectrum of interest, the X-ray scattering is inelastic and eq 12 becomes

$$I_{\mathrm{inel}} = \int \mathrm{d}t A(t) \langle \psi(t) | L |^2 \psi(t) \rangle \tag{14}$$

where the spatial averaging is carried out on the intensity level with the nonstationary wavefunction and the time dependence of $\psi(t)$ is reflected in the diffraction intensity. Equation 14 is obtained with the help of the completeness relation, $\sum_n |\phi_n\rangle\langle\phi_n = I$, where I is the identity operator.

As seen from eqs 13 and 14, the level of spatial averaging is determined by the effective elasticity, which is a measure of the relative time scale of X-ray scattering versus molecular motion. To be specific, the dynamic response defines the time scale of X-ray scattering $\delta t \propto \hbar/\delta\epsilon$. Then, for elastic scattering, the system moves so fast that an X-ray photon "sees" the complete wave function during the scattering event and hence the averaging is carried out on the amplitude level. In contract, for inelastic scattering, the system moves so slowly that an X-ray photon "sees" a frozen configuration during the scattering event and hence the averaging is carried out on the intensity level. In a sense, the distinction between elastic and inelastic scattering in X-ray and electron diffraction[17] is similar to the difference between homogeneous and inhomogeneous broadening in optical spectroscopy.

Equation 12 is the general result of our time-scale analysis, which takes into account several factors in time-resolved X-ray scattering: coherence of the X-ray source, pulse duration, and effective elasticity. In the next two sections, this general result will be applied to X-ray diffraction experiments for detecting electronic and nuclear dynamics.

III. X-ray Measurement of Electronic Dynamics in Atomic Systems

Application of eq 12 to atomic systems[18,19] or molecular systems with frozen atoms is relatively simple because the nuclear degrees of freedom are not included in the analysis. For these relatively simple systems, several cases are discussed below.

1. Inelastic Scattering. For inelastic scattering with electronic interference, the scattering intensity in eq 14 becomes

$$I_{\mathrm{inel}}(t) = \int \mathrm{d}t A(t) [N + \int \mathrm{d}\mathbf{r} \rho_2(t, \mathbf{r}) e^{i\mathbf{s}\cdot\mathbf{r}}] \tag{15}$$

where N is the number of electrons and $\rho_2(t, \mathbf{r})$ is the time-dependent two-body electron correlation function defined as

$$\rho_2(t, \mathbf{r}) = \sum_{\mu \neq \nu} \langle \psi(t) | \delta(\mathbf{r} - \mathbf{r}_\mu + \mathbf{r}_\nu) | \psi(t) \rangle_{\mathrm{ens}} \tag{16}$$

with electron indices μ and ν. The subscript ens in the above expression indicates an ensemble average which reduces $\rho_2(t, \mathbf{r})$ to the density matrix representation if the system is not in a pure state. The spatial dependence in $\rho_2(t, \mathbf{r})$ describes electronic spatial correlation, and the temporal dependence in $\rho_2(t, \mathbf{r})$ describes electronic temporal coherence. In fact, $\rho_2(t, \mathbf{r})$ can be understood as a reduced description of electronic structure and dynamics of many-electron systems. As has been demonstrated, such reduced descriptions often relate electronic responses to optical properties and hence provide a unified framework for studying electronic structures and dynamics in conjugated polymers, semiconductors, nanostructures, and biological complexes.[20] Here, ultrafast X-ray diffraction can be used to measure directly time-dependent two-body electron correlation functions.

2. Elastic Scattering. For elastic scattering, the scattering intensity in eq 13 becomes

$$I_{\mathrm{el}}(t) = \int \mathrm{d}t A(t) \sum_i \rho_i(t) |f_i|^2 \tag{17}$$

where i denotes electronic states and the time-dependent probability on the ith electronic state is $\rho_i(t) = \langle |c_i(t)|^2 \rangle_{\mathrm{ens}}$. Thus, time-resolved elastic scattering can be used to map out the time evolution of electron density and therefore provides a direct measure of electronic population relaxation.[18,19]

3. Mixed scattering. For the situation where X-ray scattering is neither elastic nor purely inelastic, the scattering intensity in eq 12 becomes

$$\mathrm{I(t)} = \int \mathrm{dtA(t)} \sum_{\mathrm{(i,j,n)}} \rho_{\mathrm{ij}}(\mathrm{t}) \mathrm{f}_{\mathrm{ni}}^{+} \mathrm{f}_{\mathrm{nj}} \tag{18}$$

where $\rho_{ij}(t) = \langle c_i(t) c_j^*(t) \rangle_{\mathrm{ens}}$ is the time-dependent density matrix and the summation indices i, j, n are constrained by the pulse duration and the dynamic response, as explained earlier. In comparison with elastic scattering, the inelastic components in the above expression introduce off-diagonal terms in the density matrix in X-ray diffraction and thus can be used to detect electronic dephasing. Both elastic and inelastic scattering are special cases of this more general expression.

It is implied in the above discussion that sub-femtosecond X-ray pulse durations are required to resolve electronic coherence among widely separated electronic states. This is no longer true when electronic states are sufficiently close, as in large molecules and Rydberg states.[18] In these cases, the interference among electronic states can be observed in ultrafast diffraction patterns when the relative phases oscillate slowly with respect to the pulse duration.

As shown above, inelastic and elastic X-ray diffraction methods provide direct measurements of electronic dynamics.[18] It should be pointed out that the contribution from inelastic X-ray scattering is more significant at large scattering angles than at small scattering angles. Considering the relatively small X-ray photon flux presently available in ultrafast X-ray diffraction experiments, X-ray detection may be presently limited to relatively small scattering angles. From this aspect, electron diffraction might be preferred since the small angle scattering is mainly inelastic.[17] Though both electrons and nuclei scatter electrons, the contribution from nuclear dynamics is a stationary background as the molecular structure is frozen on the time scale of electron dynamics.

IV. Reconstructing Molecular Dynamics from X-ray Diffraction

In this section, we specialize the general expression in eq 12 to the more complicated situation of X-ray diffraction from

molecular systems where molecular dynamics can be conveniently reconstructed from X-ray diffraction patterns.

A. Born−Oppenheimer Approximation and Nonadiabatic Effects. The general expression in eq 12 can be applied to molecular systems with the help of the Born−Oppenheimer separation of electronic from vibrational and rotational degrees of freedom. Depending on temporal and spatial resolutions, one can treat electronic (femtoseconds), vibrational (picoseconds), and rotational (nanoseconds) degrees of freedom as elastic, mixed, or inelastic scattering variables. For subpicosecond X-ray diffraction, it is reasonable to treat electrons (r) as elastic and nuclei (R) as inelastic, which agrees with the timescale separation of electronic and nuclear degrees of freedom implied in the Born−Oppenheimer adiabatic approximation.

To begin, the non-stationary wave function $\psi(t)$ is expanded as $\psi(t) = \sum_i \xi_i(t, R)\phi_i(r; R)$, where $\xi_i(t, R)$ is the nonstationary rovibrational wave function evolving on the ith electronic energy surface and $\phi_i(r; R)$ is the ith electronic eigen wavefunction solved for a given nuclear configuration R. Applying eq 13 to electronic variables and eq 14 to nuclear variables, we obtain

$$I = \sum_i \int \mathrm{d}t A(t)\langle \xi_i(t, R)|f_i(R)|^2 \xi_i(t, R)\rangle_R \qquad (19)$$

where $f_i(R)$ is the elastic electronic scattering amplitude on the ith electronic surface defined as

$$f_i(R) = \langle \phi_i(r; R)|L|\phi_i(r; R)\rangle_r \qquad (20)$$

Here again, the completeness relation for the nuclear variables is invoked to reduce the spatial averaging from the amplitude level to the intensity level. This result can be understood from the fact that the nuclear variables are frozen on the time scale of X-ray scattering, whereas the electronic variables move on a much shorter time scale. So, effectively, X-ray photons probe electrons as electron distributions and nuclei as frozen configurations, which are the main assumptions of the snapshot approach.

It should be noted that the adiabatic separation implied in eq 19 is defined with respect to the time scale of X-ray scattering. The time-scale separation in eq 19 is no longer valid when the Born−Oppenheimer approximation breaks down; then the relevant electronic variables may also become inelastic as in the case of curve crossing or closely spaced high-lying electronic surfaces.[18] Consequently, the general expression in eq 12 is needed to describe the electronic coherence in additional to nuclear dynamics. Then the X-ray scattering intensity can be expressed as

$$I = \sum_{(i,j,n)} \int \mathrm{d}t A(t)\langle \xi_i(t, R)|f_{ni}^{+}(R)f_{nj}(R)|\xi_j(t, R)\rangle_R \qquad (21)$$

where the summation over pairs of states (i, j) is constrained by the pulse duration, the summation over n is constrained by the dynamic response, with $f_{ni}(R)$ being the inelastic scattering amplitude defined as $f_{nj}(R) = \langle \phi_n(r; R)|L|\phi_j(r; R)\rangle_r$. Equation 19 is a special case of the above expression when all the electron indices are equal, $i = j = n$, and there is no interference among difference electronic states. In the simplest case of two coupled electronic surfaces, a femtosecond X-ray pulse can in principle reveal quantum beats in the crossover regime and the oscillation of the beats will be modulated by nuclear motions. Thus, ultrafast X-ray diffraction can in principle be a useful and direct way to study nonadiabatic dynamics in molecular systems.

B. Independent Atom Model. With current X-ray temporal resolution, the snapshot analysis based on eq 19 is usually sufficient to interpret and invert X-ray diffraction patterns. Within the snapshot approach, we can further simplify the analysis by invoking the independent atom model (IAM),[15] which assumes that atoms are well-localized and hence scatter X-ray photons independently. This is a reasonable assumption, because the main scattering comes from core electrons which are not sensitive to nuclear dynamics. Within this model, the elastic scattering amplitude for a molecule is approximated by a sum of localized atomic elastic amplitudes, giving

$$f_i(\mathbf{s}) = \sum_\alpha \mathrm{e}^{i\mathbf{s}\cdot\mathbf{R}_\alpha} f_i^\alpha(\mathbf{s}) \qquad (22)$$

where α is the index of atoms. Here, $f_i^\alpha(\mathbf{s})$ is the scattering amplitude from the αth atom, defined as

$$f_i^\alpha(\mathbf{s}) = \sum_\mu \mathrm{e}^{i\mathbf{s}\mathbf{r}_{\mu,\alpha}} \qquad (23)$$

where μ is the electron index on the αth atom and $\mathbf{r}_{\mu,\alpha}$ is the corresponding coordinate relative to the atomic coordinate. Then, we have

$$|f_i(\mathbf{s})|^2 = \sum_{\alpha\beta} \mathrm{e}^{i\mathbf{s}\cdot(\mathbf{R}_\alpha - \mathbf{R}_\beta)} f_i^\alpha * (\mathbf{s}) f_i^\beta(\mathbf{s}) \qquad (24)$$

in which only the interatomic separation vector $\mathbf{R}_{\alpha\beta} = \mathbf{R}_\alpha - \mathbf{R}_\beta$ appears explicitly. The key approximation in IAM is the removal of **R**-dependence in the atomic scattering amplitude, which allows for a simple relation between X-ray diffraction and nuclear dynamics.

To facilitate extracting information about nuclear dynamics from the diffraction pattern, we further ignore the **s**-dependence in the atomic scattering amplitude. This approximation allows us to follow nuclear dynamics directly from X-ray diffraction without direct reference to electron density. Substituting eq 24 into eq 19, we have

$$I(\mathbf{s}) = \int \rho(\mathbf{q})\mathrm{e}^{i\mathbf{s}\cdot\mathbf{q}} d\mathbf{q} \qquad (25)$$

where the pulse-averaged internuclear distribution function is

$$\rho(\mathbf{q}) = \int \mathrm{d}t A(t) \sum_i \langle \xi_i(t, R)| \sum_{\alpha\beta} \delta(\mathbf{q} - \mathbf{R}_{\alpha\beta}) R(f_i^\alpha f_i^\beta *)|\xi_i(t, R)\rangle_R \qquad (26)$$

with the real part R resulting from the summation over atoms. When the X-ray pulse is sufficiently short to be treated as a delta function in eq 26, the real-time molecular dynamics can thus be retrieved by measuring $\rho(\mathbf{q})$ as a function of delay time τ. Even when the X-ray pulse is not sufficiently short, the convolution in eq 26 can in principle be deconvolved to yield real-time dynamics if the pulse envelope $A(t)$ is known. The transformation between the diffraction pattern $I(\mathbf{s})$ and pulse-averaged molecular configuration $\rho(\mathbf{q})$ as defined in eq 25 is a standard diffraction inversion problem, which will be studied below.

C. Inversion for a Cylindrically Symmetric Sample. The advantage of the optical-pump and X-ray probe technique is to provide a real-time picture of molecular dynamics in real space. As is well-known, the inversion from scattering intensity to electron density can be achieved by Fourier transformation techniques provided that the phase information in the scattering amplitude can be recovered. To achieve this, enormous effort

has been devoted to invert X-ray data from **s**-space to **q**-space. It should be noted that, although the forward transformation in eq 25 is a Fourier integration in three-dimensional space, the inversion (or the backward transformation) is often carried out in a lower dimensional space. For example, the diffraction pattern of an isotropic sample has spherical symmetry so that the inversion is one-dimensional.

Optical excitation breaks the symmetry of an initially isotropic sample and produces a cylindrical distribution. Depending on the relative angle between the polarization vector ϵ of the optical pump pulse and the wave vector $\mathbf{k}_o$ of the incident X-ray beam, diffraction patterns have different angular distributions. In the parallel arrangement, where the polarization vector ϵ and the incident wave vector $\mathbf{k}_o$ are parallel, the diffraction pattern has spherical symmetry, just as for an isotropic sample. In the perpendicular arrangement, where the polarization vector ϵ and the incident wave vector $\mathbf{k}_o$ are perpendicular, the diffraction pattern is a function of both the azimuthal and scattering angles, with parity symmetry, as shown in Figure 1. For any other arrangements between these two extremes cases, there is generally no symmetry. Thus, the inversion for a cylindrical symmetric sample is a new feature due to optical pump excitation.

We begin by expressing the distribution function defined in eq 26 in polar coordinates,

$$\rho(\mathbf{q}) = \sum_l \rho_l(q)\, P_{2l}(\hat{\mathbf{q}}_z) \tag{27}$$

where, as a result of parity conservation, only even-order Legendre polynomial P_{2l} are present. The unit vector along the symmetry axis $\hat{\mathbf{z}}$ is parallel to the polarization vector of the pump pulse. In the weak response limit (i.e., single-photon absorption), the angular distribution can be truncated to the second-order Legendre polynomial, which is the case addressed by other studies. However, beyond the weak response limit (for example, in strong pumping to produce higher population of molecules undergoing dynamics) higher order Legendre polynomials are needed to describe the angular distribution resulting from multiphoton excitation.

It should be noted that the inversion becomes a standard Fourier transformation if the scattering vector **s** spans three-dimensional space. In practice, however, the diffraction pattern is measured for a fixed incident X-ray wavelength such that the scattering vector **s** is a function of the two angular variables discussed below and hence the Fourier transformation is two-dimensional in a non-Cartesian space. Substituting eq 27 into 25, we obtain the expression for the diffraction pattern

$$I(\mathbf{s}) = I(\theta, \eta) = \sum_l (-1)^l P_{2l}(\hat{s}_z) \int \rho_l(q) j_{2l}(sq) q^2 \mathrm{d}q \tag{28}$$

where $\hat{\mathbf{s}}_\mathbf{z}$ is the z-component of the scattering vector **s** whose magnitude is s and j_{2l} is the $2l$th order spherical Bessel function. The goal of inversion is to solve for $\rho_l(q)$ from eq 28 so that $\rho(\mathbf{q})$ in eq 27 can be recovered. In the parallel arrangement, $\hat{\mathbf{s}}_z = \sin(\theta/2)$, and the inversion is a one-dimensional problem, since there is no dependence on the azimuthal angle η. In the perpendicular arrangement sketched in Figure 1, the scattering vector **s** is given as

$$\mathbf{s} = s\{\cos(\theta/2)\sin(\eta), \sin(\theta/2), \cos(\theta/2)\cos(\eta)\} \tag{29}$$

with $s = 2k\sin(\theta/2)$. Therefore, $\hat{s}_z = \cos(\theta/2)\cos(\eta)$, and the resulting diffraction pattern is a function of scattering angle θ and azimuthal angle η. Because both angular variables appear in $\hat{s}_z$, the inversion cannot be expressed as the product of two separate one-dimensional transformations, as in Fourier transformation of Cartesian coordinates. Though feasible, numerical inversion on a two-dimensional grid is tedious. If the angular distribution is known, as in the weak field limit, the inversion process can simplified enormously.

For an isotropic sample or a parallel arrangement, diffraction patterns along different η angles are equivalent and give the same radial distribution function. This is no longer the case for the perpendicular arrangement for X-ray diffraction from a cylindrical sample. However, along a special direction $\hat{s}_z = 0$, (i.e., $\cos(\eta) = 0$) Legendre polynomials become constant and there is s-dependence only in the spherical Bessel functions. Using the orthogonality of spherical Bessel functions, the inversion can be accomplished along this single diffraction direction according to

$$\rho_l(q) = (-1)^l \frac{1}{4\pi P_{2l}(0)} \int_0^\infty I(\theta, \pm\pi/2) j_{2l}(sq) \frac{\mathrm{d}s}{s^2} \tag{30}$$

where $I(\theta, \pm\pi/2)$ is the diffraction along the special azimuthal angle. In practice, the integral in eq 30 is truncated at a certain s_{max} and the diffraction pattern along $\cos(\eta) = 0$ is relatively weak. Nevertheless, one-dimensional inversion in eq 30 is considerably simpler than the two dimensional inversion implied in eq 28.

D. Isolating Excited State Dynamics by Molecular "π Pulses". Since the observed diffraction pattern contains contributions from both the ground and excited states, the excited state dynamics are usually not isolated from the contamination of the ground state distribution and dynamics. In the special case that the two distributions are well separated in coordinate space, the dynamics can be separated by observing the difference. Particularly, in the weak response limit (single-photon pumping), the diffraction pattern can be fitted to a given angular distribution of zero and second spherical harmonics and thus the radial distributions from the two electronic states can be easily extracted and separated according to their different symmetries and different equilibrium radial distances.[10]

When multiphoton excitation is present, as in the strong response limit, the situation becomes more complicated because of the higher order spherical harmonics in the angular distribution. To this end, we can use the recently developed molecular "π pulse"[13,14] to isolate the excited state dynamics from the interference by the ground state distribution. Theoretical analysis has suggested that nearly complete electronic population inversion of molecules can be achieved with intense positively chirped broad-band laser pulses, as a combined result of vibrational coherence and adiabatic inversion.[13] In particular, a four-level model can be designed to illustrate for molecular systems the intriguing correlation between the sign of the chirp and the excited state population. Inversion probabilities of up to 99% have been demonstrated using strong field quantum calculations and are supported by experimental evidence. The results have been shown to be robust with respect to changes in light field parameters as well as to thermal and condensed phase conditions. In the next section, X-ray diffraction patterns of a molecular system pumped by a molecular π pulse are illustrated by an numerical example.

V. A Numerical Example

To demonstrate the transformation between evolving molecular structures and time-resolved X-ray diffraction patterns, illustrative numerical results based on I_2 molecules will be

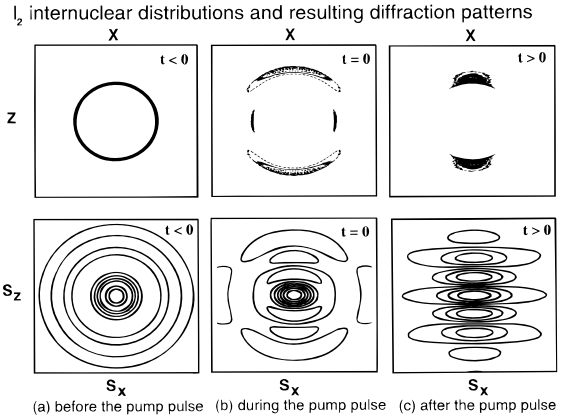

Figure 2. Contour plots of the *XZ* plane inter-nuclear distribution (top panels) and the corresponding X-ray diffraction patterns on the S_xS_z plane (bottom panels) of an initially ground state I_2 sample excited to the B state by a molecular "π pulse" of 100 fs pulse duration. The delay time between the X-ray and optical pulses is $\tau = -200$ fs (before the excitation pulse) in part a $\tau = 0$ fs (at the peak of the excitation) in part b, and $\tau = 200$ fs (after the excitation pulse) in part c.

shown in this section. The I_2 gas sample is initially in the ground electronic state and ground vibrational eigenstate and is then excited by a 100 fs fwhm molecular "π pulse" to the excited *B* electronic state. The X-ray probe pulse of 1.54 Å (Cu Kα line) is assumed to be instantaneous on the nuclear time scale but sufficiently long on the electronic time scale so that the independent atom model in eq 24 is applicable. The internuclear distribution function in eq 26 is transformed to a diffraction pattern according to eq 28, in the perpendicular arrangement. The resulting contour plots of inter-nuclear distribution functions $\rho(\mathbf{r})$ and X-ray diffraction patterns $I(\mathbf{s})$ are given in the $z-x$ plane before the pump pulse ($\tau = -200$ fs) in Figure 2a, at the peak of the pump pulse ($\tau = 0$ fs) in Figure 2b, and after the pump pulse ($\tau = 200$ fs) in Figure 2c, respectively. Before the excitation, as in Figure 2a, the nuclear wave function is isotropic and the diffraction pattern has a center of symmetry. After the excitation, as in Figure 2c, all the ground electronic state population is inverted to the excited state. In addition, the excited wave packet is aligned along the polarization direction $\hat{\mathbf{z}}$ and thus the diffraction pattern has more variation along that direction than along the perpendicular direction. During the excitation, as in Figure 2b, the wave function consists of unexcited and excited wave packets and thus the diffraction pattern is a mixture of the two. As can be seen from these figures, during the excitation, the molecular wave packet on the excited state surface becomes more localized in angular distribution but more dispersed in radial distribution. This example is different from the numerical calculations in the previous paper[10] because of optical excitation of molecular π pulses. In the strong excitation regime, the angular and radial distributions are coupled and the diffraction patterns are more complicated than those resulted from weak excitation. Further numerical studies can demonstrate the simple inversion of eq 30, electronic coherence in materials, nonadiabatic effects in molecular systems, etc.

VI. Conclusions

In this paper, we have investigated and elucidated several theoretical aspects of ultrafast X-ray diffraction, which are necessary to extend stationary X-ray theory to the time-dependent domain. The key step in our theoretical treatment is the reduction from the amplitude level to the intensity level as a consequence of photon statistics. The resulting scattering intensity can be factorized to give rise to temporal and spectral resolution. On the basis of the general formalism, several time-scale considerations are summarized below. 1. For coherent X-ray sources, the time-scale analysis on the amplitude level is sufficient. For incoherent X-ray sources, the short coherence time yields a delta function for the electric field self-correlation function and reduces the time averaging on the amplitude level in eq 2 to the time averaging on the intensity level in eq 9.

2. Because of the time averaging of the scattering intensity over the X-ray pulse duration, the coherence of the molecular wave packet excited by the optical pump pulse is not detectable between any two eigenstates when their relative phase oscillates dramatically over the duration of the X-ray pulse.

3. The observed final state of the probed molecular system ranges over a spectrum determined by the dynamic response, which is the combined effect of the resolution of X-ray detection, the range of final states with nonvanishing scattering amplitudes, and the spectral bandwidth of X-ray pulse.

4. The effective elasticity of X-ray scattering is defined based on the dynamic response for a particular dynamical variable of a molecular system. (i) If the dynamic response covers the accessible spectrum of the variable, the scattering is inelastic and is spatially averaged on the intensity level. (ii) If the dynamic response is smaller than the energy gap of of the variable, the scattering is elastic and is spatially averaged on the amplitude level. (iii) If the dynamic response couples a few states but not all states, the scattering is mixed.

It is evident that the analysis of a particular ultrafast X-ray diffraction experiment has to take into account these time-scale considerations.

As a result of this time-scale analysis, we have derived the central result of our theory, eq 12, for a general ultrafast X-ray diffraction experiment. Applying eq 12 to electronic structure and dynamics, we conclude that inelastic X-ray diffraction measures the time-dependent two electron correlation whereas elastic X-ray diffraction measures the time-dependent electronic density distribution function, given by the electronic state population.

For molecular systems, the effective elasticity is defined with respect to individual degrees of freedom. On the basis of the time-scale separation implied in the Born−Oppenheimer adiabatic approximation, the snapshot approach assumes elastic scattering for electrons and frozen configurations for nuclei. This assumption breaks down when electronic motions are coupled with nuclear motions in a curve crossing region. In this case, general analysis based on eq 21 is necessary and time-resolved X-ray diffraction patterns will demonstrate quantum beats which are modulated by nuclear motions.

It becomes clear from our analysis that the pulse duration is the crucial X-ray parameter for resolving electronic coherence and nonadiabatic dynamics. Realistic considerations of molecular time-scales lead to an estimation of subpicosecond pulse duration. In addition, experimental verification of the theoretical predictions requires improved photon flux and signal-to-noise ratio. Though not available with the current X-ray generating technology, such X-ray pulses can be expected in the near future.

Within the Born−Oppenheimer approximation, the independent atom model is adopted to reduce the general expression in eq 21 to a much simplified version in eq 24. With this simplified expression, a diffraction pattern is directly related to a time-averaged internuclear distribution function such that molecular dynamics can be directly probed without reference to electron density. The accurate inversion of the diffraction pattern of an initially isotropic sample to recover the nuclear

dynamics can be simplified greatly due to the cylindrical symmetry of optically excited molecular systems. In addition, with help of the molecular "π pulse" technique,[13,14] the excited state dynamics can in principle be isolated and investigated without contamination by the ground state distribution. It should be noted that eq 24 and the results thus obtained are invalid when the underlying assumptions are violated and thus the general treatment based on eq 21 becomes necessary.

As a natural development of optical pump−probe and stationary X-ray techniques, ultrafast X-ray diffraction and absorption experiments enable real-time measurements of evolving structures and quantum dynamics in real space. As is well-known, one can obtain a global picture of structures from X-ray diffraction or electron diffraction, a measurement of valence charge distribution from chemical shifts, an account of local environments from near-edge absorption resonances and extended absorption fine structure (EXAFS). By varying the delay time between optical pumping and the probing X-ray or electron pulse, we add a new dimension to the information obtained from such ultrafast experiments, which also present new challenges of how to interpret and invert the time-resolved observable. Though presented in the context of ultrafast X-ray diffraction, the theoretical treatments in this paper, especially these time scale considerations, can also be used to analyze other time-resolved experimental methods, including ultrafast electron diffraction[21,22] and ultrafast X-ray absorption. The detailed analysis and numerical examples of these other related time-resolved methods will be left for future studies.

Acknowledgment. We thank Larry Bartell, M. Ben-Nun, and Jianwei Che for helpful discussions.

References and Notes

(1) Róentgen, W. C. *Nature* **1896**, *53*, 274.
(2) Rentzepis, E. P. M. *Proc. SPIE* **1995**, *2521*.
(3) Srajer, V.; Teng, T. Y.; Ursby, T.; Pradervand, C.; Ren, Z.; Adachi, S.; Schildkamp, W.; Bourgeois, D.; Wulff, M.; Moffat, K. *Science* **1996**, *274*, 1726.
(4) Schoenlein, R. W.; Leemans, W. P.; Chin, A. H.; Volfbeyn, P.; Glover, T. E.; Balling, T. E.; Zolotorev, M.; Kim, K. J.; Chattopadhyay, S.; Shank, C. V. *Science* **1996**, *274*, 236.
(5) Guo, T.; Rose-Petruck, C.; Jimenez, R.; Raksi, F.; Squier, J.; Walker, B.; Wilson, K. R.; Barty, C. P. J. *Proc. SPIE* **1997**, *3157*, 84.
(6) Rischel, C.; Rousse, A.; Uschmann, I.; Albouy, O.-A.; Greindre, J.-P.; Audebert, P.; Gauthier, J.-C.; Fórdter, E.; Martin, J.-L.; Antonetti, A. *Nature* **1997**, *390*, 490.
(7) Wark, J. *Contemp. Phys.* **1996**, *37*, 205.
(8) Raksi, F.; Wilson, K. R.; Jiang, Z.; Ikhlef, A.; Cote, C. Y.; Kieffer, J.-C. *J. Chem. Phys.* **1996**, *104*, 6066.
(9) Bergsma, J. P.; Coladonato, M. H.; Edelsten, P. M.; Kahn, J. D.; Wilson, K. R.; Fredkin, D. R. *J. Chem. Phys*. **1986**, *84*, 6151.
(10) Ben-Nun, M.; Cao, J.; Wilson, K. R. *J. Phys. Chem.* **1997**, *101*, 8743.
(11) Cao, J.; Wilson, K. R. *Proc. SPIE* **1998**, 3273. In press.
(12) Lin, S. H.; Chao, C. H.; Ma, H.; Rentzepis, P. M. *Proc. SPIE* **1995**, 2521.
(13) Cao, J.; Bardeen, C.; Wilson, K. R. *Phys. Rev. Lett*. **1998**, *80*, 1406.
(14) Cao, J.; Bardeen, C.; Wilson, K. R. *J. Chem. Phys.* **1998**. Submitted for publication.
(15) Agarwal, B. K. *X-ray Spectroscopy: An Introduction*; Springer-Verlag: Berlin, 1991.
(16) Murnane, M. M.; Kapteyn, H. C.; Falcone, R. W. *Phys. Rev. Lett*. **1989**, *62*, 155.
(17) Bonham, R. A.; Fink, M. *High Eergy Electron Scattering*; Van Norstrand Reinhold Company: New York, 1974.
(18) Krause, J. L.; Schafer, K. J.; Ben-Nun, M.; Wilson, K. R. *Phys. Rev. Lett*. **1997**, *79*, 4978.
(19) Ben-Nun, M.; Martinez, T. J.; Weber, P. M.; Wilson, K. R. *Chem. Phys. Lett*. **1996**, *262*, 405.
(20) Mukamel, S.; Tretiak, S.; Wagersreiter, T.; Chernyak, V. *Science* **1997**, *277*, 781.
(21) Williamson, J. C.; Zewail, A. H. *Proc. Natl. Acad. Sci. U.S.A.* **1991**, *88*, 2766.
(22) Elsayed-Ali, H. E.; Weber, P. M. In *Time-Resolved Electron and X-ray Diffraction*; Rentzepis, P. M., Helliwell, J., Eds.; Oxford Press: New York, 1995.